Structure and Dynamics of Bacteriophage IKe Major Coat Protein in MPG Micelles by Solution NMR†

Karen A. Williams,‡,§ Neil A. Farrow,|| Charles M. Deber,*,§ and Lewis E. Kay*,||

Division of Biochemistry Research, Hospital for Sick Children, Toronto M5G 1X8 and Department of Biochemistry, University of Toronto, Toronto M5S 1A8, Ontario, and Protein Engineering Network Centres of Excellence and Departments of Medical Genetics, Biochemistry and Chemistry, University of Toronto M5S 1A8, Ontario, Canada

Received December 8, 1995; Revised Manuscript Received February 16, 1996⊗

ABSTRACT: The structure and dynamics of the 53-residue filamentous bacteriophage IKe major coat protein in fully protonated myristoyllysophosphatidylglycerol (MPG) micelles were characterized using multinuclear solution NMR spectroscopy. Detergent-solubilized coat protein (sequence: AEPNAATNYATEAMD-SLKTQAIDLISQTWPVVTTVVVAGLVIRLFKKFSSKAV) mimics the membrane-bound "assembly intermediate" form of the coat protein which occurs during part of the phage life cycle. NMR studies of the IKe coat protein show that the coat protein is largely α-helical, exhibiting a long amphipathic surface helix (Asn 4 to Ser 26) and a shorter "micelle-spanning" C-terminal helix which begins at Trp 29 and continues at least to Phe 48. Pro 30 likely occurs in the first turn of the C-terminal helix, where it is ideally situated given the hydrogen bonding and steric restrictions imposed by this residue. The similarity of ^{15}N relaxation values (T_1, T_2, and NOE at 500 MHz and T_2 at 600 MHz) among much of the N-terminal helix and all of the TM helix indicates that the N-terminal helix is as closely associated with the micelle as the TM helix. The description of the protein in the micelle is supported by the observation of NOEs between lysolipid protons and protein amide protons between Asn 8 and Ser 50. The N-terminal and TM helices exhibit substantial mobility on the microsecond to second time scale, which likely reflects changes in the orientation between the two helices. The overall findings serve to clarify the role of individual residues in the context of a TM α-helix and provide an understanding of the secondary structure, dynamics, and aqueous and micellar environments of the coat protein.

Solution NMR[1] studies of small membrane proteins in detergent micelles have yielded valuable insights into the structure and dynamics of membrane proteins [reviewed in Henry and Sykes (1994) and Opella et al. (1994)]. The filamentous bacteriophage major coat proteins, such as those belonging to M13 and Pf1, have long been employed as model membrane proteins by virtue of their small size and the ease with which pure phage can be obtained in large quantities. The secondary structure of M13 (Henry & Sykes, 1992; van de Ven et al., 1993) and Pf1 (McDonnell et al., 1993) consists of two helical regions corresponding to an N-terminal amphipathic helix and a C-terminal hydrophobic helix. The N-terminal helix is predicted to lie at the membrane interface (McDonnell et al., 1993), perpendicular to the hydrophobic helix which spans the micelle (Henry & Sykes, 1992). The presence of an amphipathic surface helix and a transmembrane (TM) helix is characteristic of many integral membrane proteins, e.g., the light harvesting complex from *Rhodopseudomonas acidophila*, the structure of which was recently determined to high resolution using X-ray crystallography (McDermott et al., 1995).

However, the high-resolution structure of a micelle-bound phage coat protein and the detailed interactions of the protein with the lipid environment have yet to be determined. The structural characterization of coat proteins by NMR is complicated by the fact that, unlike soluble proteins where the relative orientation of secondary structural elements is defined by long range protein−protein contacts, in the case of proteins with extensive membrane-interactive regions the relative orientation of structural elements is determined to a large extent by detergent−protein interactions. A detailed understanding of this complex system requires that these interactions be characterized. In addition, a description of the dynamics of the protein should also be included. Solution NMR techniques provide a powerful tool with which to characterize protein motions on a wide range of time scales (i.e., from picosecond to second).

The present application of high resolution solution NMR methods to bacteriophage IKe major coat protein in myris-

* Address correspondence to either of these authors.
‡ Present address: European Molecular Biology Laboratory, Meyerhofstrasse 1, Postfach 10.2209, 69012 Heidelberg, Germany.
§ Hospital for Sick Children and Department of Biochemistry.
|| Protein Engineering Network Centres of Excellence and Departments of Medical Genetics, Biochemistry, and Chemistry.

† This work was supported, in part, by grants to C.M.D. and L.E.K. from the Medical Research Council of Canada. K.A.W. held a Medical Research Council Studentship. N.A.F. is a Research Fellow of the National Cancer Institute of Canada supported with funds provided by the Canadian Cancer Society.
⊗ Abstract published in *Advance ACS Abstracts,* April 1, 1996.

[1] Abbreviations: (HB)CBCACO(CA)HA, α/β proton to α/β carbon to carbonyl correlation; CBCA(CO)NH, α/β proton to α/β carbon (via carbonyl carbon) to nitrogen to amide proton correlation; HMQC, heteronuclear multiple-quantum coherence; HNCACB, amide proton to nitrogen to α/β carbon correlation; HNCO, amide proton to nitrogen to carbonyl carbon correlation; HSQC, heteronuclear single-quantum coherence; MPG, myristoyllysophosphatidylglycerol; NMR, nuclear magnetic resonance; NOE, nuclear Overhauser effect; gd-HCCH-TOCSY, gradient enhanced proton−carbon−carbon−proton correlation using carbon total correlated spectroscopy; SEDUCE, selective decoupling using crafted excitation; TM, transmembrane.

0006-2960/96/0435-5145$12.00/0

toyllysophosphatidylglycerol (MPG) micelles extends previous NMR studies of the coat proteins by characterizing specific interactions between the coat protein and micellar and aqueous environments. The lysolipid MPG was employed since it closely resembles a biological membrane lipid but forms micelles because of the presence of a single acyl chain. IKe coat protein itself had not previously been characterized and is ideal for study by virtue of its monomeric state and thermostability (Williams & Deber, 1993). In the present study, the backbone and side chain chemical shift assignments of the IKe coat protein in MPG micelles are determined, together with the elucidation of the secondary structure of the protein and the establishment of a number of intermolecular contacts between lipid and protein. In addition, backbone dynamics are characterized from measurement of ^{15}N relaxation rates and analyzed using a model-free approach (Lipari & Szabo, 1982a,b). Together, the protein secondary structure, dynamics, and interactions with the lysolipid environment provide a detailed description of a membrane protein in a micelle.

EXPERIMENTAL PROCEDURES

Sample Preparation. Uniformly isotopically labeled IKe coat protein was obtained by propagating the phage in the *Escherichia coli* prototroph JM101/pCU109 in the minimal media defined below containing [^{15}N]ammonium sulfate (MSD Isotopes, Merck Frosst Canada Inc., Montreal, Quebec), and with [$^{13}C_6$]glucose for double-labeled samples. IKe was unable to infect bacteria grown in the widely used minimal media M9 or M63 (Sambrook et al., 1989; Henry et al., 1986), and, as a result, it was necessary to develop a more complete medium, MIM (cytidine, 100 mg; guanosine, 100 mg; adenine, 100 mg; uridylic acid, 100 mg; $Na_3C_6H_5O_7 \cdot 2H_2O$, 535 mg; $MnSO_4 \cdot H_2O$, 0.164 mg; $CaCl_2 \cdot 2H_2O$, 3.81 mg; $ZnSO_4 \cdot 7H_2O$, 0.04 mg; $FeCl_2 \cdot 4H_2O$, 3.6 mg; $CuSO_4 \cdot 5H_2O$, 0.05 mg; NaCl, 0.5 g; KNO_3, 100 mg; Na_2HPO_4, 6.0 g; NaH_2PO_4, 0.5 g; KCl, 0.25 g; KH_2PO_4, 3.0 g; thiamine HCl, 5.0 mg; 1 M $MgSO_4$, 1.0 mL; 20% glucose, 10.0 mL; $(NH_4)_2SO_4$, 2 g; bring to 1 L, stir, and sterilize by filtration).

Phage was harvested upon the addition of PEG/NaCl and purified on a KBr step gradient (Williams & Deber, 1996). NMR samples were prepared by adding 6.6 mg of purified phage (uniformly ^{15}N or ^{15}N,^{13}C labeled) in 1 mL of TE buffer (10 mM Tris, 1 mM EDTA, pH 8) to 1 mL of either 200 mM protonated myristoyllysophosphatidylglycerol (MPG) or [^2H]myristoyl[^1H]lysophosphatidylglycerol (MPG) (Avanti Polar Lipids, Inc., Alabaster, AL) in 5 mM NaCl and 5 mM sodium borate. The coat protein was extracted upon addition of 200 μL of $CHCl_3$, which was removed by evaporation upon shaking at 200 rpm for 2 h at 37 °C, and then lyophilized. The sample was solubilized with 0.5 mL of 95% H_2O/5% D_2O and the pH adjusted just prior to use to make a 2 mM coat protein sample in 400 mM MPG, pH 4.5. The DNA and the minor coat proteins present in the sample have been shown not to interfere with the biophysical characterization of the major coat protein (Williams & Dunker, 1977; Dunker et al., 1991).

NMR Spectroscopy. NMR experiments were recorded at 45 °C on Varian UNITY 500 and UNITY+ 600 MHz spectrometers equipped with pulsed field gradient units and triple-resonance probes with actively shielded *z*-gradients. All spectra were recorded in fully protonated MPG in H_2O except where noted. Experiments involving amide proton detection used pulsed field gradients for coherence transfer pathway selection (Kay et al., 1992; Schleucher et al., 1993; Muhandiram & Kay, 1994) making use of an enhanced sensitivity approach (Cavanagh et al., 1991; Palmer et al., 1991) with minimal H_2O saturation and dephasing (Grzesiek & Bax, 1993; Stonehouse et al., 1994; Kay et al., 1994). The following numbers of complex points and acquisition times were employed in the experiments used in the present study: 2D $^1H-^{15}N$ HSQC (Kay et al., 1992; Bodenhausen & Ruben, 1980) ^{15}N (F_1) 128, 77.6 ms, NH (F_2) 512, 64 ms (8 transients); HNCO (Kay et al., 1990, 1994) ^{13}CO (F_1) 64, 42.7 ms, ^{15}N (F_2) 26, 23.3 ms, NH (F_3) 512, 64 ms (16 transients); HNCACB (Wittekind & Mueller, 1993) $^{13}C^{\alpha}/^{13}C^{\beta}$ (F_1) 32, 4.2 ms, ^{15}N (F_2) 32, 23.3 ms, NH (F_3) 512, 64 ms (48 transients); CBCA(CO)NH (Grzesiek & Bax, 1992) $^{13}C^{\alpha}/^{13}C^{\beta}$ (F_1) 52, 6.6 ms, ^{15}N (F_2) 32, 23.3 ms, NH (F_3) 512, 64 ms (28 transients); (HB)CBCACO(CA)HA (Kay, 1993) $^{13}C^{\alpha}/^{13}C^{\beta}$ (F_1) 52, 7.1 ms, ^{13}CO (F_2) 64, 42.7 ms, H^{α} (F_3) 512, 64 ms (16 transients). A pulsed field gradient HCCH-TOCSY (Kay et al., 1993) spectrum was recorded (16 scans) on a sample of IKe in 95% H_2O with a mixing time of 16 ms with the following acquisition parameters; ^1H (F_1) 96, 34.3 ms, ^{13}C (F_2) 32, 10.7 ms, ^1H (F_3) 512, 64 ms. A simultaneous ^{15}N-,^{13}C-edited NOESY spectrum (Pascal et al., 1994) was recorded (16 scans) employing a mixing time of 150 ms and acquisition parameters of ^1H (F_1) 128, 20.0 ms, $^{13}C/^{15}N$ (F_2) 32, 10.7 ms, ^1H (F_3) 416, 52 ms. ^{15}N-NOESY-HSQC (Zuiderweg & Fesik, 1989; Marion et al., 1989a) and TOCSY-HSQC (Marion et al., 1989b) spectra were recorded (16 scans) using the enhanced sensitivity pulsed field gradient and "water flip-back" methods as described by Zhang et al. (1994). Acquisition parameters of ^1H (F_1) 110, 20.0 ms, ^{15}N (F_2) 32, 21.3 ms, ^1H (F_3) 512, 64 ms were employed, and in the case of the NOESY experiment mixing times of 75 and 150 ms were used. In the case of the TOCSY spectrum, a mixing time of 40 ms was employed using a DIPSI-2rc mixing scheme (Cavanagh & Rance, 1992) to eliminate the contributions from cross relaxation in the rotating frame (Griesenger et al., 1988). An F_1-filtered, F_3-edited ^{13}C NOESY-HMQC (Lee et al., 1994) was recorded (32 scans) with a mixing time of 150 ms and acquisition parameters of ^1H (F_1) 50, 12.5 ms, ^{13}C (F_2) 32, 10.7 ms, ^1H (F_3) 512, 64 ms.

Typical carrier positions employed in the double- and triple-resonance experiments were 119.5 ppm for ^{15}N, 178.0 ppm for ^{13}CO, 58 ppm for $^{13}C^{\alpha}$, 43 ppm for $^{13}C^{\alpha}/^{13}C^{\beta}$ (i.e., aliphatic carbons), and 4.58 ppm for ^1H. Experiments in which protons directly bound to nitrogen were detected during acquisition employed WALTZ-16 ^{15}N decoupling (Shaka et al., 1983), while experiments which detected aliphatic protons during acquisition made use of GARP for ^{13}C decoupling (Shaka et al., 1985). Where necessary (e.g., HNCACB), carbonyl decoupling was achieved using a SEDUCE-1 ^{13}C decoupling sequence centered at 178 ppm (McCoy & Mueller, 1992).

The 150 ms simultaneous ^{15}N-,^{13}C-edited NOESY experiment was performed on an IKe sample dissolved in ^2H-myristoyl-^1H-lysophosphatidylglycerol, 95% H_2O, 5% D_2O while the F_1-filtered, F_3-edited ^{13}C NOESY-HMQC was recorded on a sample dissolved in [^2H]myristoyl[^1H]-lysophosphatidylglycerol, D_2O, using the pulse sequence in

Lee et al. (1994), with the exception that the filtering and editing steps were reversed. All other experiments were recorded on samples of ^{1}H-MPG, 95% H_2O, 5% D_2O.

Quadrature detection in all of the indirectly detected dimensions was achieved via States−TPPI (Marion et al., 1989c). Spectra were processed using the NMRPipe software system (Delaglio et al., 1995) and analyzed with the peak picking program PIPP (Garrett et al., 1991). Postacquisition solvent suppression was employed in all spectra where NH protons were detected (Marion et al., 1989d). In the case of the simultaneous ^{15}N-,^{13}C-edited NOESY experiment, a time domain deconvolution procedure was employed as described previously (Muhandiram et al., 1993) to remove the residual water peak from the spectrum. For constant time ^{15}N evolution periods, mirror image linear prediction was used to extend the time domain signal (Zhu & Bax, 1990), while forward−backwards linear prediction methods (Zhu & Bax, 1992) were employed in the case of nonconstant time ^{15}N evolution periods.

Amide Exchange. A series of 2D ^{1}H−^{15}N HSQC spectra were collected at intervals beginning 8 min after the addition of D_2O to a 1 mM ^{15}N-labeled IKe coat protein and 400 mM ^{1}H-MPG sample. Spectra were initially recorded every 5 min. Spectral acquisition times were increased as the interval between experiments was increased (i.e., as cross peak intensities decreased). Peak intensities were subsequently normalized to account for the differences in the number of transients between the various spectra, and the time dependence of the intensities fit to a simple exponential decay function to extract the exchange rate at each of the slowly (lifetimes on the order of minutes) exchanging NH positions.

^{15}N Backbone Relaxation. A series of inverse detected two-dimensional ^{1}H−^{15}N NMR experiments were employed to determine backbone ^{15}N T_1 and T_2 relaxation times and heteronuclear ^{1}H−^{15}N steady-state NOE values at 500 MHz and T_2 values at 600 MHz (Kay et al., 1989; Farrow et al., 1994a, 1995). ^{1}H−^{15}N HSQC spectra of IKe established the presence of two distinct cross peaks for the Trp 29 indole and the amide (^{15}N,NH) of Gln 27. Exchange cross peaks connecting the two sites for Trp 29 and Gln 27 were observed when ^{1}H−^{15}N correlation experiments were recorded with a mixing time inserted between the ^{15}N chemical shift evolution and proton detection periods (Farrow et al., 1994b). In order to measure ^{15}N relaxation times, T_1 and T_2, as well as to determine the slow conformational exchange rates, pulse schemes were employed in which the ^{15}N chemical shift was recorded prior to the periods in which either longitudinal or transverse nitrogen magnetization is allowed to decay. A description of the schemes employed is provided in Farrow et al. (1994b). The enhanced sensitivity pulse scheme of Farrow et al. (1994a) was employed to measure steady-state ^{1}H−^{15}N NOE values.

T_1, T_2, and NOE spectra were recorded as 160 × 512 complex matrices with 64 scans per complex t_1 point and with spectral widths of 1650 and 8000 Hz in F_1 and F_2, respectively. Recycle delays of 1 s were employed in both the T_1 and T_2 experiments. The T_1 experiment was recorded with eight delays T [see Figure 1 of Farrow et al. (1994b)] of 10, 110, 220, 360, 690, 920, and 1200 ms, while the eight delays in the T_2 experiment were T 16, 32, 48, 64, 80, 96, 112, and 144 ms. ^{1}H−^{15}N NOE values were determined from two spectra, recorded with and without ^{1}H saturation. A recycle delay of 6 s was employed for the spectrum recorded in the absence of ^{1}H saturation, while a 3 s recycle delay followed by a 3 s period of ^{1}H saturation was employed in the NOE experiment. The intensities of peaks in the two-dimensional spectra were characterized from peak heights, and ^{1}H−^{15}N steady-state NOE enhancements were calculated as the ratio of peak heights obtained in the presence and absence of proton saturation. T_1 and T_2 times were determined from a nonlinear least-squares fit of an exponential curve to the measured data as described previously (Farrow et al., 1994a). In the case of data from the Trp 29 indole and the amide ^{15}N of Gln 27, a more complex analysis of peak intensities is needed in order to extract both the T_1 relaxation times and the exchange rates characterizing the interconversion between the two states (Farrow et al., 1994b).

The relaxation properties of an amide ^{15}N nucleus are dominated by the dipolar interaction with its attached proton and by chemical shift anisotropy (CSA), and the T_1, T_2, and NOE values are given by Abragam (1961) as

$$1/T_1 = (d^2/4)[J(\omega_H - \omega_N) + 3J(\omega_N) + 6J(\omega_H + \omega_N)] + c^2 J(\omega_N) \quad (1)$$

$$1/T_2 = (d^2/8)[4J(0) + J(\omega_H - \omega_N) + 3J(\omega_N) + 6J(\omega_H) + 6J(\omega_H + \omega_N)] + (c^2/6)[3J(\omega_N) + 4J(0)] \quad (2)$$

$$\mathrm{NOE} = 1 + (\gamma_H/\gamma_N)(d^2/4)[6J(\omega_H + \omega_N) - J(\omega_H - \omega_N)]T_1 \quad (3)$$

In eqs 1−3, $d = [\mu_0\gamma_H\gamma_N h/(8\pi^2)]\langle 1/r^3_{NH}\rangle$ and $c = (\omega_N/\sqrt{3})(\sigma_{||} - \sigma_\perp)$ where h is Planck's constant, γ_H and γ_N are the gyromagnetic ratios of the ^{1}H and ^{15}N nuclei respectively, ω_H and ω_N are the ^{1}H and ^{15}N Larmor frequencies, r_{NH} is the internuclear ^{1}H−^{15}N distance (1.02 Å), $\sigma_{||}$ and $\sigma_\perp$ are the parallel and perpendicular components of the (assumed) axially symmetric ^{15}N chemical shift tensor, and $J(\omega)$ is the value of the spectral density function at frequency ω. Equations 1−3 show that T_1, T_2, and NOE values are dependent on the values of the spectral density function at five frequencies. Since the number of observables (T_1, T_2, and NOE) is insufficient to explicitly determine the values of the spectral density function at all five frequencies, the method of Lipari and Szabo (1982a,b) was employed to characterize the rates and amplitudes of motion of individual NH bond vectors via

$$J(\omega) = (2/5)[S^2\tau_m/(1 + \omega^2\tau_m{}^2) + (1 - S^2)\tau/(1 + \omega^2\tau^2)] \quad (4)$$

In eq 4, τ_m is the overall correlation time of the molecule, τ_e is the correlation time characterizing internal motions on times scales much faster than the overall correlation time with $\tau^{-1} = \tau_m{}^{-1} + \tau_e{}^{-1}$, and the generalized order parameter, S, describes the degree of spatial restriction of motion. The model-free spectral density function given in eq 4 assumes that the overall tumbling motion of the molecule is isotropic; the validity of this assumption for the IKe coat protein in an MPG micelle is addressed below. An additional parameter, R_{ex}, may also be employed to represent contributions to the ^{15}N transverse relaxation rate arising from motions occurring on time scales much slower (millisecond to microsecond)

than the overall rotational correlation time according to

$$1/T_2 = 1/T_{2(DD)} + 1/T_{2(CSA)} + R_{ex} \quad (5)$$

where $1/T_{2(DD)}$ and $1/T_{2(CSA)}$ are the contributions to the transverse relaxation rate from dipolar and CSA relaxation mechanisms, respectively. The values of S^2, τ_e, and R_{ex} chacterizing the dynamics of individual residues may be obtained from eqs 1−5 once the value of τ_m has been determined. The overall correlation time τ_m may be estimated from the ratio of T_1/T_2 assuming that $\tau_e < 100$ ps, $\tau_m > 1$ ns, and the absence of chemical exchange (Kay et al., 1989). A better approach, however, is to determine the optimum value of τ_m by simultaneously fitting all of the measured relaxation data using eqs 1−5 and employing a grid search in τ_m. In the present case the global optimum in τ_m was obtained by fitting T_1, T_2, and $^1H-^{15}N$ NOE values measured at 500 MHz (^1H frequency) and the T_2 values obtained at 600 MHz assuming a form of the spectral density function given by eq 4 and including the effects of exchange with a parameter, R_{ex}. Note that R_{ex} is scaled in a manner proportional to the square of the field at which the T_2 measurements were recorded [i.e., $R_{ex}^{600} = (36/25)R_{ex}^{500}$]. In this way the contributions from exchange which would otherwise lead to an overestimate in τ_m are minimized. Once a global optimum τ_m has been selected, the experimental data may then be fit using a variety of spectral density functions including the two time scale spectral density model proposed by Clore et al. (1990),

$$J(\omega) = (2/5)[S^2\tau_m/(1 + \omega^2\tau_m^2) + (S_f^2 - S^2)\tau/(1 + \omega^2\tau^2)] \quad (6)$$

where $S^2 = S_f^2S_s^2$. In eq 6, S_f^2 and S_s^2 describe the amplitudes of internal motions occurring on fast and slow time scales, respectively, and $\tau^{-1} = \tau_m^{-1} + \tau_s^{-1}$, with τ_s the correlation time for the slow internal motions. The optimal form of the spectral density function was selected as described previously (Farrow et al., 1994a).

RESULTS

Sample Conditions. Heteronuclear NMR experiments require the incorporation of isotopic labels into the protein by growth in minimal media containing [^{13}C]glucose and/or [^{15}N]ammonium sulfate or chloride. IKe failed to grow in the common minimal media M9 or M63, although these media sustain the growth of bacteriophage M13 as well as *E. coli.* As a result, we developed a more complete defined medium (MIM) in which IKe grows almost as well as in rich media (see Experimental Procedures).

The dispersion in the $^1H-^{15}N$ correlation spectrum of uniformly ^{15}N-labeled wild type IKe coat protein in 400 mM perdeuterated SDS is slightly poorer than that obtained for M13 and fd coat proteins in SDS (Henry & Sykes, 1992; van de Ven et al., 1993; McDonnell et al., 1993). The spectra of each of the proteins exhibits the limited chemical shift dispersion characteristic of helical proteins. SDS does not possess a lipid head group and was therefore not appropriate for this study since one of the principal objectives was to characterize the interactions between the protein and both the head group and acyl chain of the detergent. Lysolipids are also excellent membrane mimetics since they occur in biological membranes and carry a lipid head group but form micelles because they possess only a single acyl chain.

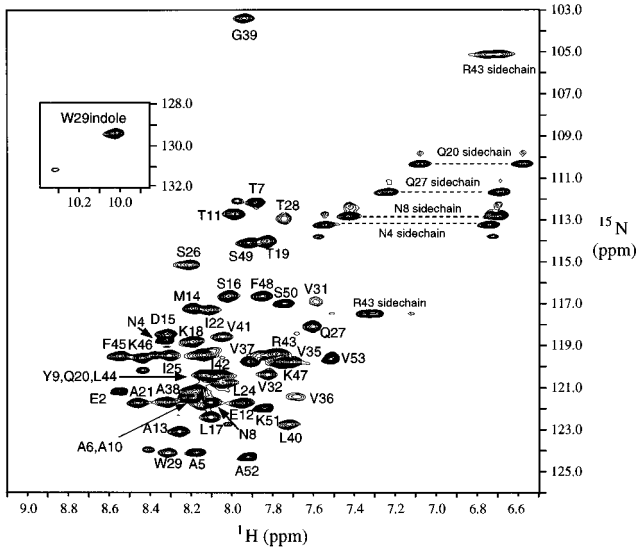

FIGURE 1: $^1H-^{15}N$ HSQC spectrum of 2 mM ^{15}N-labeled wild-type IKe coat protein in 400 mM ^1H-MPG, 95% H_2O, 5% D_2O, pH 4.5, 45 °C. The Arg 43 (R43) side chain resonances are folded. Note the presence of major and minor peaks associated with the Trp 29 (W29) indole. The sequence of the 53-residue protein is AEPNAATNYATEAMDSLKTQAIDLISQTWPVV-TTVVVAGLVIRLFKKFSSKAV.

To determine the most suitable lysolipid to solubilize the coat protein, $^1H-^{15}N$ correlation spectra of IKe coat protein in a variety of fully protonated lysolipids (400 mM) were examined (not shown). The lysolipids included the net neutral lauryllysophosphatidylcholine (^1H-LPC), the negatively charged myristoyllysophosphatidylglycerol (^1H-MPG), and mixtures of the two. Chemical shift dispersion was poor in ^1H-LPC but improved upon addition of ^1H-MPG, and while a 40% MPG/60% LPC mixture appeared satisfactory, 100% MPG was selected for subsequent study because resonances were slightly better resolved (Figure 1). Spectra were recorded at 45 °C and pH 4.5 in accord with previous coat protein studies [e.g., 50 °C for fd studies at pH 4.0 (McDonnell & Opella, 1993); 37−39 °C for M13 at pH 5.1 (van de Ven et al., 1993); and 45 °C for M13 at pH 4.5 (Henry & Sykes, 1992)]. Approximately 50 well-resolved amide resonances were detected in the $^1H-^{15}N$ HSQC spectrum. Although this number is consistent with the number of amide protons in the protein, it was subsequently determined that a number of the peaks represented minor species (see below). A high detergent concentration (400 mM) was employed to prevent doubling of many of the cross peaks which was observed for the M13 coat protein at low detergent concentrations (Henry & Sykes, 1992; van de Ven et al., 1993) as well as to enhance protein stability. Note that unlike what was observed by van de Ven et al. (1993) the line widths of peaks associated with the minor species did not differ noticeably from the line widths of the corresponding peaks originating from the major species.

In contrast to all previous studies of membrane proteins in micelles, many of the experiments were carried out with 400 mM fully protonated lysolipid. The use of 400 mM ^1H-MPG in these studies of the IKe coat protein was made possible by the incorporation of pulsed field gradients to select for coherence transfer pathways which include ^{15}N in experiments which detect NH protons. Pulsed field gradients

were also used to help suppress signals arising from the lipid (^{1}H−^{12}C) in favor of protein signals (^{1}H−^{13}C). However, in experiments which detect magnetization arising from aliphatic protons, pulsed field gradients were not used to select for coherence transfer pathways, since in general this approach results in unacceptable sensitivity losses for methyl and methylene groups (Kay et al., 1992; Muhandiram & Kay, 1994). Although protonated lysolipid was suitable for the majority of experiments, NOESY spectra detecting aliphatic and aromatic protons [simultaneous ^{15}N−^{13}C-edited NOESY-HSQC (Pascal et al., 1994), F_1-filtered, F_3-edited ^{13}C NOESY-HMQC (Lee et al., 1994)] were recorded on samples dissolved in [^{2}H]myristoyl[^{1}H]lysophosphatidylglycerol to eliminate noise which would otherwise be present due to subtraction artifacts from intense signals associated with the lipid. Additionally, the use of [^{2}H]myristoyl[^{1}H]lysophosphatidylglycerol minimized magnetization loss stemming from spin diffusion involving lysolipid acyl chain protons. Many of the protein resonances remained weak, however, in the presence of [^{2}H]myristoyl[^{1}H]lysophosphatidylglycerol, suggesting that processes other than ^{1}H−^{1}H spin flips between protein protons and lipid protons—such as slow conformational exchange—contribute to line broadening (see below).

Resonance Assignments. The backbone and side chain assignments were obtained from a series of triple-resonance correlation experiments which exploit large heteronuclear scalar couplings to establish connectivities between nuclei. This strategy was employed because of amino acid degeneracy in the coat protein (e.g., Val 31−Val 37) and poor dispersion, although this approach is typically reserved for much larger proteins [e.g., Ikura et al. (1990)]. A triple-resonance approach readily facilitated the backbone assignment of the M13 coat protein in ^{2}H-SDS (van de Ven et al., 1993), which had previously been assigned in part using a combination of selective labeling, pH titrations, and proteolytic cleavage (Henry & Sykes, 1992).

Backbone ^{15}N, NH, ^{13}C$^\alpha$, and ^{13}C$^\beta$ assignments were determined from the CBCA(CO)NH experiment (Grzesiek & Bax, 1992), which correlates backbone ^{15}N and NH resonances with ^{13}C$^\alpha$ and ^{13}C$^\beta$ resonances of the preceding residue, and the HNCACB experiment (Wittekind & Mueller, 1993), which correlates the ^{13}C$^\alpha$ and ^{13}C$^\beta$ resonances of the preceding residue with intraresidue backbone ^{15}N, NH, ^{13}C$^\alpha$, and ^{13}C$^\beta$ resonances (Figure 2a). The distinctive ^{13}C$^\alpha$ and ^{13}C$^\beta$ shifts of Ala, Gly, Ser, and Thr lead to the immediate identification of these residues so that they served as the starting points for assignment (e.g., the Ala 38-Gly 39 locus). The degeneracy of Val in the transmembrane (TM) region made unambiguous assignment of these residues difficult. Amide resonances from residue Ala 1 to Ile 22, and from Leu 44 to Val 53, were intense in comparison to weak resonances between these regions, a phenomenon which may stem in part from slow conformational exchange (e.g., Asp 23−Trp 29, see below) or from rapid relaxation caused in part by the proximity to acyl chain protons (e.g., Val 31−Val 37). The CBCA(CO)NH and HNCACB spectra facilitated assignment of the majority of the backbone resonances, with most remaining ambiguities resolved by two additional experiments, viz., the HNCO (Figure 2b) (Kay et al., 1990, 1994), which establishes connectivities between the amide chemical shift with the CO of the preceding residue, and the (HB)CBCACO(CA)HA (Figure 2c) (Kay, 1993), which correlates intraresidue C$^{\alpha/\beta}$, CO, and H$^\alpha$ shifts. The HNCO experiment was particularly useful in cases where resonances have similar ^{15}N and NH shifts (e.g., Ala 6 and Ala 10; Asp 15 and Asn 4. See in Figure 2b). The sensitivity of the HNCO experiment also confirmed the presence of numerous minor species in addition to the major species (e.g., Asn 8 in Figure 2b). The (HB)CBCACO(CA)HA experiment provided H$^\alpha$ assignments for residues Ala 1−Ala 21 and Arg 43−Val 53, while residues Ile 22−Val 42 were not detected. The ^{15}N and NH chemical shifts for Asp 23 and Thr 34 and the nitrogen chemical shift of Thr 33 were not assigned.

Side chain ^{13}C and ^{1}H assignments were carried out using the simultaneous ^{15}N,^{13}C-edited NOESY experiment (Pascal et al., 1994) in [^{2}H]myristoyl [^{1}H]lysophosphatidylglycerol, the ^{15}N-NOESY-HSQC in ^{1}H-MPG (Zhang et al., 1994), and the ^{13}C gd-HCCH-TOCSY experiment in ^{1}H-MPG (Kay et al., 1993). The ^{13}C gd-HCCH-TOCSY experiment allowed identification of residue type and side chain assignment by correlating the ^{1}H and ^{13}C shifts of one (^{13}C,^{1}H) pair with the ^{1}H shift(s) of other intraresidue protons. Sequential and short-range NOEs (Figure 3) are consistent with the assignments (Supporting Information).

A number of residues exhibited minor species in addition to the principal component, including Ala 1 (e.g., indicated by "*" in Figure 2c), Glu 2 (two minor peaks), Asn 4, Ala 5, Ala 6, Thr 7 (two minor peaks), Asn 8 (see Figure 2b), Gln 27, Trp 29 indole, and Gly 39. Several of the minor peaks corresponding to residues at the termini of the protein were in fact more intense than many of the resonances of residues in the hydrophobic TM segment. The only exchange peaks between major and minor species involved the Trp 29 indole and the Gln 27 backbone amide (see below). The origin of the remaining minor species is not clear; however, N-terminal amino acid sequencing confirmed that the extra peaks do not arise from heterogeneous N-terminal processing.

Secondary Structure. IKe coat protein is largely helical in MPG micelles on the basis of sequential and short-range NOEs (Figure 3a) and chemical shift deviations from random coil (Figure 4) (Wishart & Sykes, 1994). Sequential NH NOEs characteristic of α-helical conformation were observed throughout the entire protein beginning at Asn 4 and extending through to Ala 52. Helical conformation is further supported by the presence of αN (i,i+3) NOEs. NOEs in a number of regions, including the Val-rich TM helix, were ambiguous due to chemical shift overlap among these residues.

Chemical shift deviations from random coil offer additional insight into the conformation of the coat protein (Figure 4). The C$^\alpha$, H$^\alpha$, and CO secondary shifts are consistent with the presence of helical conformation in the region from Ala 6 to Ala 21 and Thr 34 to Lys 47. Secondary shifts (particularly the ^{15}N chemical shift of Trp 29) suggest that residues Thr 28, Trp 29, and Pro 30 are not in a helical conformation. On the basis of NOEs summarized in Figure 3, short-range side chain NOEs (not shown), and secondary shifts, the amphipathic surface helix likely begins at Asn 4 and extends through to Ser 26, while the TM helix likely begins at Trp 29 and continues at least as far as Phe 48 (see Discussion).

Backbone Dynamics. (a) Measured Relaxation Times. Values of T_1, T_2, and the steady-state ^{1}H−^{15}N NOE at 500

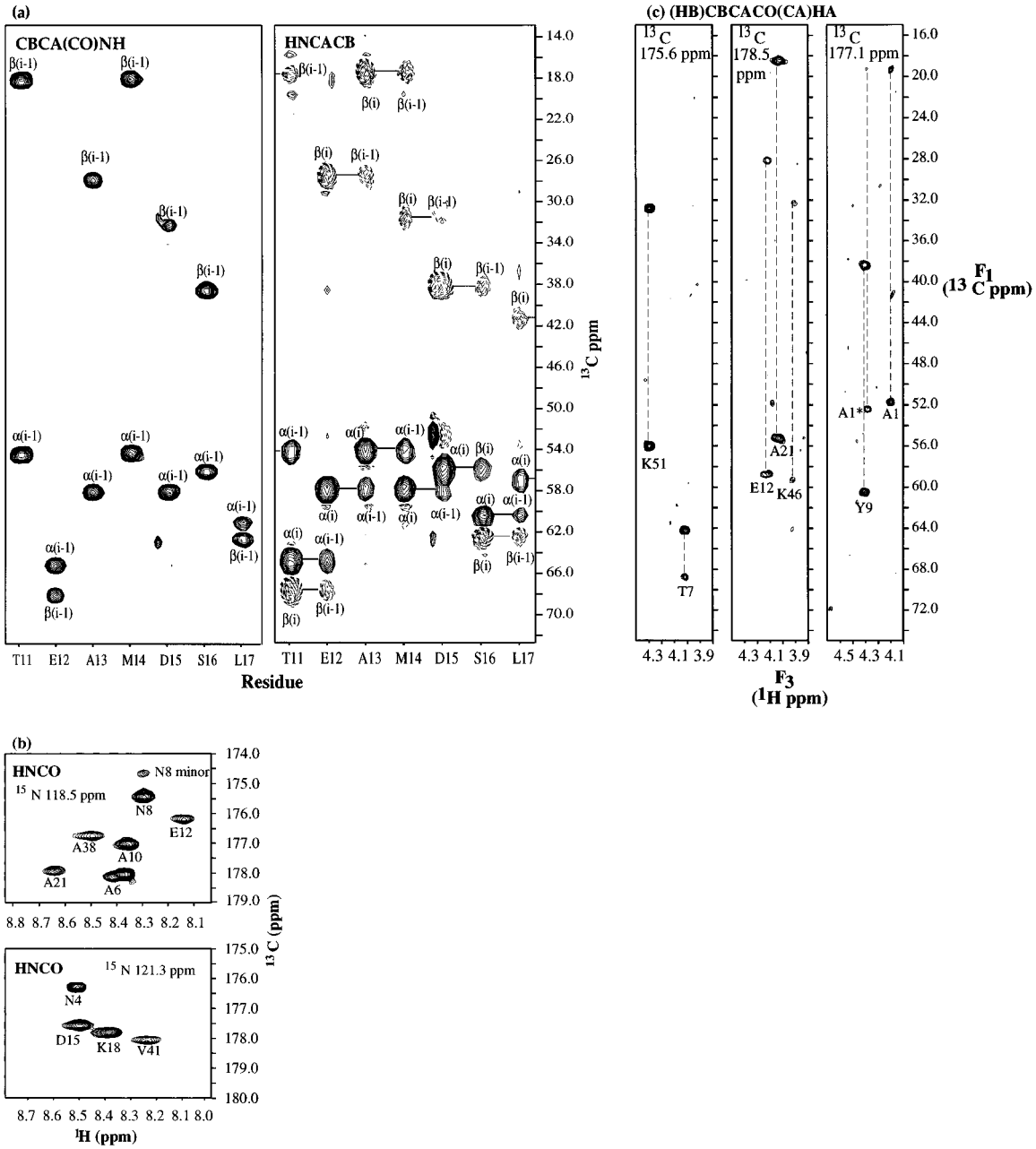

FIGURE 2: Sequential strips taken from different slices ($F_2 = {}^{15}N$) of (a) 3D CBCA(CO)NH and 3D HNCACB spectra corresponding to residues Thr 11−Leu 17 of wild-type IKe coat protein. (b) Slices from the 3D HNCO at $^{15}N = 118.5$ ppm and $^{15}N = 121.3$ ppm. (c) Slices from the 3D (HB)CBCACO(CA)HA spectrum at carbonyl chemical shifts 175.6, 178.5, and 177.1 ppm. The dotted line connects intraresidue C^{α} and C^{β} peaks. Note the appearance of an additional set of cross peaks for Ala 1, indicated with a "*". All spectra were recorded on a sample of ^{13}C,^{15}N−labeled wild-type IKe coat protein in 400 mM ^{1}H-MPG micelles, 95% H_2O, 5% D_2O, pH 4.5, 45 °C.

MHz and T_2 at 600 MHz (Figure 5) were determined as described above. The average T_1 relaxation time was 784 ms at 500 MHz. The average value of T_2 between residues Thr 11 and Phe 48 was 44 ms at 500 MHz and 40 ms at 600 MHz. T_2 relaxation times increased dramatically to ca. 300 ms from Ser 49 to Val 53 (C-terminal residues) and somewhat more gradually in the N-terminal region from Asn 8 toward Glu 2. The steady-state NOEs ranged from large negative values at the protein termini as shown by very intense negative peaks for Glu 2, Asn 4, Ala 5, Ala 52, and Val 53 to values of 0.4−0.7 between Thr 11 and Phe 48. T_2 and NOE values for residues between Thr 11 and Phe 48 show little variation, suggesting that these residues, which encompass both the N-terminal amphipathic and C-terminal helices, possess very similar dynamics. This implies that much of the *N*-terminal amphipathic helix (beginning at Thr 11) is at least as closely associated with the micelle as the hydrophobic helix.

(b) Estimation of the Overall Correlation Time. The value of the overall correlation time was determined to be 16 ns for residues Asn 8 to Phe 48 by simultaneously fitting all of the measured relaxation data using eqs 1−5. Residues at the termini of the protein were fit better with small values of τ_m (3−10 ns). The dramatically different values of τ_m at the termini suggest that these residues are not bound to the surface of the micelle. The relative uniformity of ^{15}N relaxation parameters for residues between Thr 11 and Phe 48 suggests that the assumption of isotropic overall tumbling for this portion of the protein is reasonable.

(*c) Model-Free Analysis.* The relaxation parameters (T_1, T_2, and NOE) obtained at 500 MHz, and T_2 at 600 MHz, were fit independently using five spectral density models

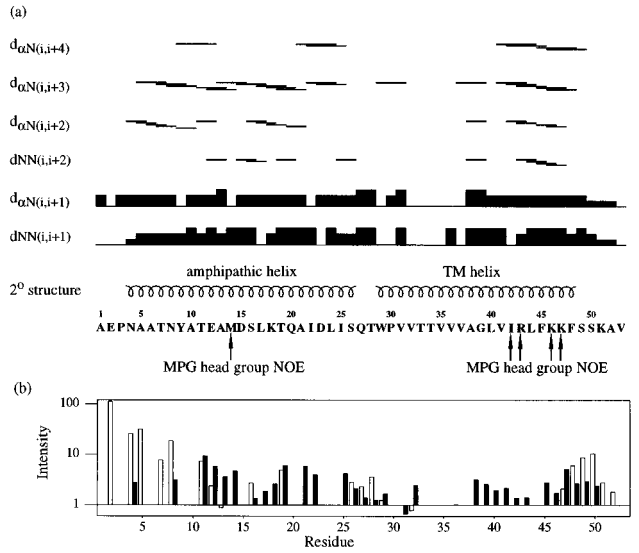

FIGURE 3: (a) Summary of sequential and short-range NOEs involving backbone NH and H$^{\alpha}$ atoms. "2° structure" refers to the predicted secondary structure of the IKe coat protein based on NOEs (including short-range side chain NOEs obtained from the simultaneous ^{15}N-^{13}C-edited NOESY) and chemical shifts. (b) Aqueous and lysolipid environments of IKe coat protein. Open bars correspond to the presence of amide exchange peaks at the water chemical shift, while closed bars indicate the presence of lysolipid methylene NOEs (1.23 ppm). Intensities determined from peak height in the 150 ms 3D ^{15}N-NOESY-HSQC experiment. All intensities were divided by 10^5. In both panels a and b, data corresponding to residues Asn 4 and Asp 15, Ala 6 and Ala 10, Tyr 9, Gln 20, and Leu 44 were ambiguous due to chemical shift overlap. Data were largely absent or ambiguous in the region surrounding Thr 33 and Thr 34, although this region is most likely helical in conformation.

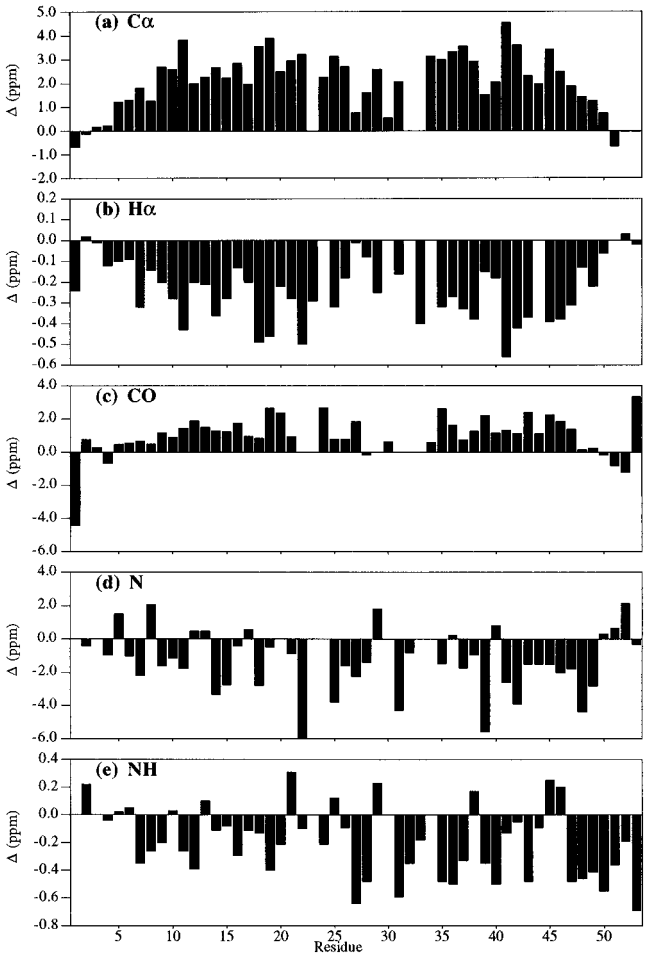

FIGURE 4: Chemical shift deviations from random coil values for backbone (a) C$^{\alpha}$, (b) H$^{\alpha}$, (c) CO, (d) ^{15}N, and (e) NH resonances. Deviations from the random coil chemical shift value occur when a residue is present in elements of secondary and tertiary structure; H$^{\alpha}$, ^{15}N, and NH resonances experience an upfield shift when located in an α-helix and a downfield shift when present in a β-sheet, while C$^{\alpha}$ and CO resonances are shifted downfield when present in an α-helix and upfield when located in a β-sheet (Wishart & Sykes, 1994; Wishart et al., 1992, 1995).

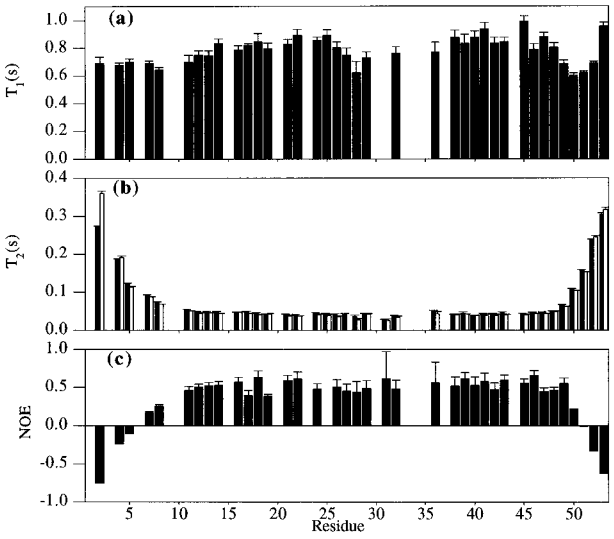

FIGURE 5: Plots of (a) T_1 (500 MHz), (b) T_2 (500 MHz, dark shaded boxes, and 600 MHz, open boxes), and (c) NOE (500 MHz) as a function of residue number.

which optimized the following combinations of parameters: S^2; S^2 and τ_e; S^2 and R_{ex}; S^2, τ_e, and R_{ex}; S_s^2, S_f^2, and τ_s (Farrow et al., 1994a). Of the 36 residues between Glu 2 and Val 53 for which complete relaxation data were obtained, 24 residues were fit using the model which included S^2, τ_e, and R_{ex}, while two were fit with S^2 and τ_e and 10 residues were fit with the two time scale model (Supporting Information). The average value of the order parameter S^2 was determined to be 0.85, similar in magnitude to values observed in helices of soluble proteins. Low values of order parameters were observed for residues in the region between the N-terminal amphipathic and C-terminal helices (most notably at Thr 28), indicating that the region between the helices has above average disorder. The average value of τ_e was 0.7 ns, considerably larger than values typically observed in elements of secondary structure in soluble proteins (i.e., 0.02 ns), suggesting that internal motions in much of the IKe coat protein are slower than motions in other folded proteins. A conformational exchange term (R_{ex}) was required to fit the data of almost every residue between Glu 12 and Phe 48 (Figure 6), with the average value of R_{ex} (500 MHz) equal to 3.6 s^{-1}.

(d) Conformational Exchange As Reported by the Trp 29 Indole and Gln 27 Backbone Cross Peaks. The use of ^{1}H−^{15}N correlation experiments which facilitate simultaneous determination of T_1 times and chemical exchange rates (Farrow et al., 1994b) demonstrated the presence of exchange peaks correlating major and minor forms of Trp 29 and Gln 27. The Trp indole resonances are well-separated in both ^{1}H and ^{15}N dimensions so that exchange rates could be accurately determined, whereas overlap between the "auto peaks" and "cross peaks" for Gln 27 prevented exchange

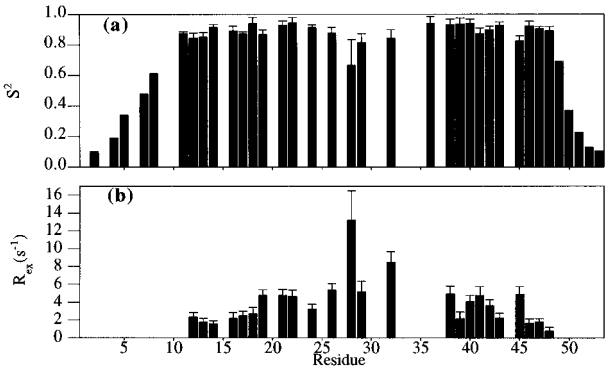

FIGURE 6: Plots of (a) S^2 and (b) R_{ex}, calculated from T_1, T_2, and NOE values obtained at 500 MHz and T_2 values at 600 MHz as a function of residue number. A value of 16 ns was used for τ_m, and the values of R_{ex} correspond to the contributions to the ^{15}N line widths from microsecond to millisecond time scale motions measured at 500 MHz (^{1}H frequency).

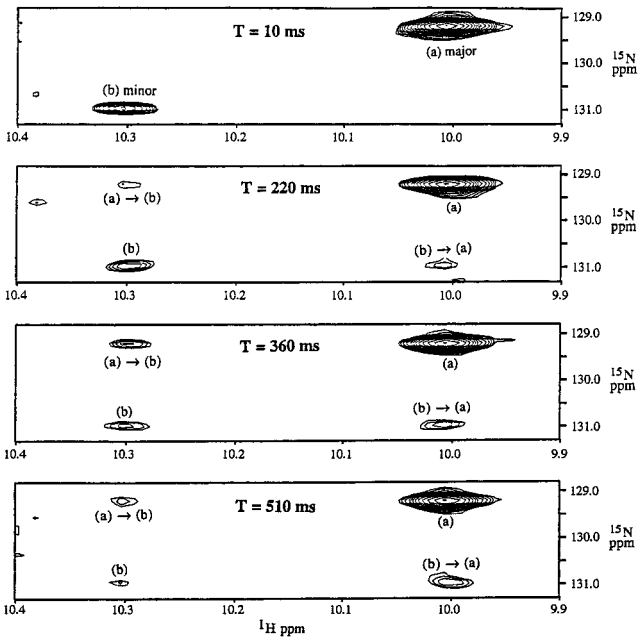

FIGURE 7: Regions of ^{1}H−^{15}N correlation spectra obtained using the pulse sequence for the simultaneous measurement of longitudinal ^{15}N decay rates and chemical exchange rates (Farrow et al., 1994b) showing exchange at the Trp 29 indole position at $T = 10$, 220, 360, and 510 ms. The equilibrium constant [M]/[m] (M = major species, and m = minor species) is 10. The spectra were recorded with 2 mM ^{15}N-labeled wild-type IKe coat protein in 400 mM ^{1}H-MPG at pH 4.5, 45 °C.

rate determination. In Figure 7, the major and minor auto peaks observed in the first spectrum ($T = 10$ ms) give rise to cross peaks in experiments with longer delays (i.e., $T =$ 220, 360, 510 ms). The cross peaks represent magnetization which was labeled with the ^{15}N chemical shift of the site of origination and the ^{1}H chemical shift of the destination site as a result of chemical exchange during the delay, T. The equilibrium constant was determined to be 10 from the ratio of the intensity of the auto peaks under fully relaxed conditions. In a system in which there is slow conformational exchange, the relaxation of the auto peaks is biexponential since the rate of decay depends on both the T_1 and exchange rates (Farrow et al., 1994b). The decay of the auto peaks as well as the buildup and decay of the cross peaks is illustrated in the Supporting Information. Values of both the decay and exchange rates were extracted by fitting a

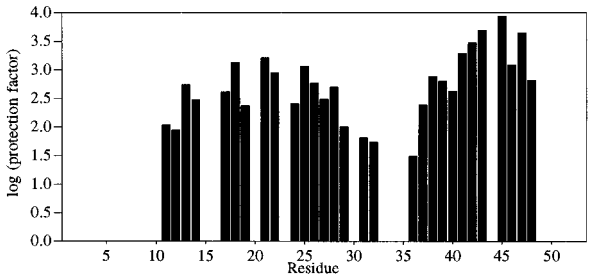

FIGURE 8: Amide exchange protection factors calculated using the method of Bai et al. (1993) as a function of residue for the IKe coat protein in 400 mM ^{1}H-MPG at pH 4.5, 45 °C.

series of equations describing the relaxation of a system undergoing exchange between two sites to the measured decay and buildup curves using a nonlinear least-squares procedure (Farrow et al., 1994b). The value of T_1 determined for the major species was 600 ms, and the exchange rate for the transition from major to minor species was 0.28 s^{-1}, while the exchange rate for the transition from minor to major species was 2.84 s^{-1}. The Trp 29 major and minor species were also present in ^{1}H−^{15}N correlation spectra of the wild type IKe coat protein in SDS and LPC micelles as well as in MPG micelles at 35 °C, although the minor species was less prominent at the lower temperature.

A number of explanations are possible to account for the observation of two distinct species involving Trp 29. The two species may originate from Trp 29 indole ring flips (rotations about the C^α−C^β and/or C^β−C^γ bonds) or alternatively Pro 30 *cis*−*trans* isomerization or some other conformational interconversion at the X-Pro imide. The exchange rates at the Trp 29 indole are consistent with *cis*−*trans* isomerization since the rate of X-Pro isomerization in soluble proteins varies from several seconds to fractions of a second depending, in part, upon adjacent residues (Brandts et al., 1975). The minor Trp 29 indole species was not observed in ^{1}H−^{15}N HSQC spectra of IKe mutants at the Pro 30 locus (Pro 30 → Ala, Pro 30 → Gly) as well as for a mutant outside this locus (Val 37 → Gly) (Williams & Deber, 1996). In contrast to Trp 29, the doubling of cross peaks observed for the other residues for which there is no evidence of slow conformational exchange in wild type IKe (e.g., Ala 1, Glu 2, and Asn 4, see above) was also observed in the HSQC spectra of the IKe mutants (Williams & Deber, 1996).

(e) Amide Exchange. Amide protection factors for the IKe coat protein in MPG micelles are illustrated in Figure 8. The exchange rates of the IKe coat protein amides are in general faster than those associated with stable helices of soluble proteins or those previously reported for the M13 coat protein in SDS micelles (Henry & Sykes, 1992). This increased rate of exchange likely reflects an effect of the lysolipid since MPG has a hydroxyl-rich head group (phosphodiglycerol) which may enhance amide exchange rates. The magnitude of protection from amide exchange was higher for residues in the C-terminal helix than in the amphipathic helix.

DISCUSSION

Coat Protein Conformation. On the basis of NOEs and secondary shifts, the IKe coat protein in MPG micelles is almost entirely helical with the amphipathic helix beginning at Asn 4 or Ala 5 and continuing at least to Ser 26. The TM helix begins at Trp 29 and continues through to Phe 48.

The presence of slow exchange between major and minor components at Gln 27 and Trp 29 and the small secondary shifts for residues between the two helices suggest that the turn region (Gln 27−Trp 29) is less structured and likely samples a range of conformations. The turn is situated in a heterogeneous environment, as shown by the presence of both amide exchange peaks with water as well as NOEs from methylene protons on the lysolipid acyl chain (Figure 3b).

The first turn of the N-terminal amphipathic helix is likely capped by Asn 4 (*i*) and is followed by Thr 7 at the *(i+3)* position, both of which can form side chain hydrogen bonds to backbone amides. The presence of side chains which can form reciprocal hydrogen bonds back to the main chain is widely observed in the first turn of helices in soluble proteins and is described as a helix capping box where the side chain of the N-cap residue (*i*) forms an hydrogen bond to the backbone NH of residue *(i+3)*, and the side chain of residue *(i+3)* forms an hydrogen bond to the NH of the N-cap residue (Harper & Rose, 1993). The most common sequence for the capping box is Ser-X-X-Glu, although the Asn-X-X-Thr sequence which occurs twice in the IKe coat protein (Asn 4−Thr 7 and Asn 8−Thr 11) has been observed to form a capping box in soluble proteins solved to high resolution (Harper & Rose, 1993). The pattern of $^{13}C^{\alpha}$ chemical shift deviations from random coil for residues Asn 4−Thr 7 is consistent with those observed for helix capping boxes in soluble proteins (Gronenborn & Clore, 1994).

On the basis of NOE connectivities and secondary chemical shifts (Figures 3a and 4), the amphipathic helix likely extends to Ser 26 and the TM helix begins at Trp 29. In this regard, it is not surprising to find a proline residue (Pro 30) in the first turn of the TM helix. Proline frequently occurs at the N-cap+1 position of helices in soluble proteins (MacArthur & Thornton, 1991; Richardson & Richardson, 1988) and is enriched in the N-terminal region flanking the TM helix in single-span membrane proteins (Landolt-Marticorena et al., 1993). The presence of Pro (*i*) in the first turn of a helix is ideal for two reasons. First, because proline lacks an amide proton, it does not require a hydrogen-bonding partner. Second, the occurrence of proline at position *(i)* generally prevents the hydrogen bond from occurring at the NH of residue (*i*+1) to the carbonyl of residue (*i*−3), which is again favorable in the first turn since this hydrogen-bond would not be satisfied anyway. This suggests that the Val 31 NH would not be hydrogen-bonded, although it could potentially hydrogen-bond with the Thr 28 side chain. The X-Pro backbone imide is more polar than other peptide bonds (Veis & Narwrot, 1970) so that the (*i*-1) carbonyl has an enhanced tendency to accept and form strong hydrogen-bonds (Deber et al., 1990). As a result, the hydrogen-bond between the Trp 29 carbonyl and Thr 33 amide proton would be expected to be particularly strong.

The conformation of the IKe coat protein is generally similar to that of other coat proteins, with the most striking difference being the length of the N-terminal amphipathic helix. This helix is considerably longer in IKe (23 residues from Asn 4 to Ser 26) than in M13 [e.g., Pro 6−Glu 20 (van de Ven et al., 1993); Ala 7−Thr 19, Gly 23−Ala 25 (Henry & Sykes, 1992)]. Although this difference reflects, in part, the fact that the IKe coat protein is longer (53 residues) than the M13 coat protein (50 residues), the amphipathic helix of the IKe coat protein begins closer to the N-terminus in IKe (possibly stabilized by the putative Asn 4-X-X-Thr 7 capping box) and extends further toward the TM helix. The turn region connecting the amphipathic and TM helices of the M13 coat protein is predicted to include Ile 22 since no sequential connectivities (NH *i*,*i*+1) were observed at this residue (van de Ven et al., 1993). The homologous residue in IKe (Ile 25) likely participates in the last turn of the N-terminal amphipathic helix since (*i*,*i*+3) connectivities are observed up to Ser 26, while the turn between the two helices is mediated by the polar residues Gln 27 and Thr 28. The TM helix has been variously defined as extending from Tyr 24 to ca. Ser 47 or Ser 50 in the M13 coat protein (Henry & Sykes, 1992; van de Ven et al., 1993). The TM helix is somewhat shorter in IKe since it begins at Trp 29 and continues to Phe 48. The residues preceding Trp 26 in the M13 coat protein are considerably less polar (21-YIGYA**W**A-27) than the corresponding residues in the IKe coat protein (24-LISQT**W**P-30). The presence of Trp 29 in the first turn of the TM helix suggests that Trp 29 is more solvent-exposed in the IKe coat protein than Trp 26 in the M13 coat protein, a notion which is supported by the intrinsic Trp fluorescence spectra of the IKe coat protein in DOC micelles in which Trp 29 resides in a polar environment (Williams & Deber, 1996). It is possible that the apparent differences in the length of the helix may result from the use of different detergents in these studies. Although both MPG and SDS are anionic, they differ in acyl chain lengths (14 vs 12), head group size, and chemistry. The orientation of the amphipathic and TM helices with respect to each other is complicated by their relative mobility. Based on solid-state NMR studies of the fd coat protein in lipid bilayers (McDonnell et al., 1993; Cross & Opella, 1979, 1981, 1985), the amphipathic helix of the fd coat protein is predicted to be oriented perpendicular to the TM helix.

Coat Protein Environment. Protein−solvent (lysolipid and water) interactions were characterized by examining NOEs between solvent and protein in a 3D enhanced sensitivity pulsed field gradient ^{15}N-NOESY-HSQC experiment (Zhang et al., 1994). In a previous study of the M13 coat protein solubilized with 20% ^{1}H-SDS and 80% ^{2}H-SDS, NOEs from SDS methylene protons to residues Ala 25, Trp 26, Val 33, and Gly 34 of the M13 coat protein were observed (Papavoine et al., 1994). Studies using spin-labeled 5- and 16-doxylstearate probes led to the suggestion that the SDS micelle is distorted near the C-terminus as a result of the interaction of Lys side chains with the sulfate head groups of the detergent (Papavoine et al., 1994). The present study of the IKe coat protein in MPG micelles extends these observations since NOEs from acyl methylene protons to amide protons were observed for almost every residue between Asn 8 and Ser 50, as summarized in Figure 3b. These NOEs stem from the very large population of degenerate lysolipid methylene protons (ca. 8 M) resonating at 1.23 ppm. Previous NOESY studies of phosphatidylcholine vesicles (Ellena et al., 1985) have demonstrated that spin diffusion can result in the efficient transfer of magnetization among all lipid protons, even at short mixing times. While spin diffusion is likely operative in the IKe/MPG micelle system considered here, it should be noted that the intensities of lipid−NH cross peaks were significantly different for different residues. Rather than interpret these NOEs in a quantitative manner, we have chosen to compare intensities of lipid−NH NOEs and NH−amide exchange with water to

get a qualitative picture of the arrangement of protein and lipid in this system, as indicated in Figure 3b.

Putative NOEs between the protons on the protein side chains and protons attached to the lysolipid head group—which are much less abundant than acyl chain protons—were also identified. To unambiguously assign protein−lysolipid head group NOEs, an F_1-filtered, F_3-edited ^{13}C NOESY-HMQC experiment was carried out on a sample in which the lipid acyl chain was perdeuterated, while the head group was protonated. In this experiment only magnetization originating from $^{1}H-^{12}C$ (the lysolipid headgroup) and detected on protons bound to ^{13}C (the protein) was observed. Specific lysolipid head group−protein NOEs were observed involving the side chains of Ile 42, Arg 43, Lys 46, and Lys 47 in the C-terminal region of the TM helix and involving Met 14 in the N-terminal amphipathic helix. The presence of protein−lysolipid head group NOEs to Met 14 in the N-terminal amphipathic helix further supports the assertion that the amphipathic helix is closely associated with the micelle. Numerous other NOEs were observed at Thr, Val, Ala, and Ile side chain methylene and methyl resonances, residues which are enriched in the TM region (e.g., 31-VVTTVVVA-GLI-42) but for which specific assignments could not be made due to overlap. ^{1}H and ^{13}C resonance assignments of the lipid established that the majority of the lysolipid head group NOEs involved the methylene protons of the carbon atom in the glycerol backbone which directly participates in the ester linkage with the acyl chain.

The absence of lysolipid methylene NOEs at the first few N- and C-terminal amide residues of the coat protein indicates that these residues are not in close contact with the micelle (Figure 3b). At the same time, these terminal residues are shown to be exposed to the aqueous milieu on the basis of amide exchange with water (Figure 3b). The pattern of lysolipid NOEs and amide exchange values in Figure 3b provides a description of the orientation of the protein with respect to the micelle by indicating interactions with solvent. The amphipathic surface helix exhibits lipid NOEs and partial protection from amide exchange from ca. Asn 8 to Thr 19. In contrast, Ile 22 and Ile 25 are more protected from amide exchange and exhibit strong lysolipid NOEs, suggesting that this region is sequestered within the hydrophobic region of the micelle. Residues predicted to be in the turn region (Ser 26 to Trp 29) exhibit both lipid NOEs and exchange with water, indicating that these residues are more exposed to the aqueous environment. The N-terminal residues of the TM helix are partially protected from amide exchange and also exhibit lipid NOEs, while the C-terminus of the helix shows NOEs to lipid with an absence of NH exchange peaks, demonstrating that this region is sequestered within the hydrophobic core of the micelle. The pattern of amide exchange peaks with water in the C-terminal portion of the protein indicates that the TM helix emerges from the micelle around Ser 49.

The most slowly exchanging amides in the M13 coat protein are from Met 28 to Phe 42 (Henry & Sykes, 1992), suggesting that these residues are likely to be at least partially sequestered within the core of the micelle. The magnitude of protection from amide exchange in the IKe coat protein is less than that observed in the M13 coat protein and on average is greater in the TM helix than in the N-terminal amphipathic helix (Figure 8). As discussed, the enhanced rate of amide exchange relative to the M13 coat protein dissolved in SDS may stem from the hydroxyl-rich environment of the MPG head group. It is possible, as well, that the IKe coat protein resides in a more polar environment than the M13 coat protein, reflecting the occurrence of hydrophilic residues surrounding Trp 29 in the IKe coat protein, compared to those in the vicinity of Trp 26 in the M13 coat protein.

The MPG-IKe coat protein interactions can be interpreted in terms of (a) nonspecific lysolipid interactions reflecting a dynamic micellar structure and (b) stable electrostatic interactions between the side chains of positively charged residues and the negatively charged head group of MPG. Like the membrane−aqueous interface of a lipid bilayer, the micelle−aqueous interface is heterogeneous as a result of thermal motions. The membrane interface can easily accommodate a helix (10 Å diameter) (White & Wimley, 1993) and can induce secondary structure formation because of the restriction of motion which is compensated energetically by the interaction of nonpolar side chains with the hydrophobic core of the membrane (Jacobs & White, 1989). The micelle can similarly be viewed as a dynamic complex with a wide heterogeneous interfacial region composed of a mixture of H_2O, the lysolipid or detergent head group, the acyl carbonyl, and methylenes (Ben-Shaul & Gelbart, 1994). The orientation of the IKe coat protein with respect to the MPG micelle is determined by the balance between the association of nonpolar protein side chains with the hydrophobic core of the micelle (hydrophobic effect) and the behavior of the surrounding lysolipids ("micelle effect") which are described as the hydrophobic and "bilayer effects", respectively, in the context of a lipid bilayer (Wimley & White, 1993). Although the MPG micelle is an excellent membrane mimetic in terms of the amphipathic environment and dynamics of the interface, other features are not as typical of a lipid bilayer, including the curvature of the micelle.

The presence of stable electrostatic interactions between the side chains of positively charged residues and the negatively charged lysolipid MPG is supported by the presence of NOEs between the C-terminal residues Arg 43, Lys 46, and Lys 47 and the lysolipid glycerol backbone. The methylenes of Arg and Lys side chains favor the nonpolar core of the micelle while the positively charged amino group of Lys and the guanidino moiety of Arg prefer to interact with lipid head groups so that these residues are ideally suited for the interface (Ballesteros & Weinstein, 1992). The presence of a cluster of positively charged residues at the cytoplasmic interface is an important topological determinant of TM helices (von Heijne, 1994).

Coat Protein Dynamics and Conformational Exchange. Although phage coat protein dynamics in micelles have been extensively characterized (Henry & Sykes, 1990), the work presented herein is the first to systematically determine the backbone ^{15}N relaxation values (T_1, T_2, and NOE) throughout the entire protein using inverse-detected two-dimensional correlation experiments (Kay et al., 1989; Farrow et al., 1994a). The region from Thr 11 to Phe 48, which encompasses part of the amphipathic helix and all of the hydrophobic TM helix, exhibits restricted motion compared to the much more mobile ends. This implies that the majority of the N-terminal amphipathic helix (beginning at Thr 11) is no more flexible than the TM helix, suggesting that both the N-terminal and the TM helices are closely associated with the micelle. In comparison, studies of the M13 coat

protein led to the suggestion that the N-terminal helix is generally more flexible on the basis of ^{15}N line widths of 5−10 Hz compared to line widths of 15−20 Hz obtained for residues in the TM helix (van de Ven et al., 1993). Although the amphipathic helix of the IKe coat protein begins at Asn 4, the region from Asn 4 to Ala 10 exhibits greater flexibility than the remainder of the surface helix. The first and last five residues of the M13 coat protein are highly mobile in contrast to the remainder of the protein (Henry et al., 1986; Leo et al., 1987; Bogusky et al., 1988; Henry & Sykes, 1992, 1990). The dynamics of fd coat protein in micelles are similar to that observed in bilayers (Leo et al., 1987).

IKe coat protein undergoes slow conformational exchange between two species as indicated by the presence of exchange peaks between major and minor species of Trp 29 (indole) and Gln 27 (backbone amide) (Figure 7). Exchange may arise from interconversions at the Trp-Pro locus, a notion which is supported by the occurrence of only a single Trp 29 indole species in HSQC spectra of IKe mutants Pro 30 → Ala and Pro 30 → Gly (Williams & Deber, 1996). Nonetheless, the Val 37 → Gly IKe mutant also gave rise to only a single Trp indole species. The Trp-Pro dipeptide is exclusively present in the *trans* conformation in a survey of soluble proteins (Stewart et al., 1990; MacArthur & Thornton, 1991), and in some systems the presence of an aromatic residue preceding Pro produces a 10-fold reduction in the isomerization rate (Brandts et al., 1975). The M13 coat protein exhibited two peaks of about equal intensity for many of the resonances between Ile 22 and Lys 48, which were interpreted in terms of an asymmetric dimer (Henry & Sykes, 1990, 1992). Chemical shift differences between the corresponding cross peaks were small except for the Trp 26 and Ala 27 backbone amides. Both Trp 26 and Ala 27 were shown to undergo slow conformational exchange (ca. 1 s) (Henry & Sykes, 1990; 1992), very much like the exchange observed at the Trp 29 position in the IKe coat protein. The Pro-mediated *cis* and *trans* isomers of calbindin were confirmed by the presence of $H^{\alpha}(i-1)$−Pro $H^{\alpha}(i)$ and $H^{\alpha}(i-1)$−Pro $H^{\delta}(i)$ NOEs, respectively, observed using 2D NMR (Chazin et al., 1989). It was not possible to assign Pro 30 H^{δ}, and therefore the isomeric state(s) of the X-Pro bond in the IKe protein could not be determined unequivocally.

In addition to the slow exchange observed at the Trp 29 and Gln 27 positions (∼second time scale), the IKe coat protein in MPG micelles also appears to undergo additional slow motions (microsecond to millisecond time scale) on the basis of chemical exchange shortened T_2 times observed for residues Thr 11−Phe 48. This may stem from changes in the orientation of the two helices with respect to each other. Unlike soluble proteins which are stabilized by very specific (generally hydrophobic) contacts between noncontiguous parts of the protein, the phage coat protein does not have tertiary protein−protein contacts in the micelle-bound form. Instead, the hydrophobic surfaces of the IKe coat protein are sequestered by the nonpolar acyl chains of the detergent in the micelle. The acyl chains of the lysolipid are highly disordered with a density similar to that of a liquid alkane, while the head group is more conformationally restricted (Attwood & Florence, 1983). A 2D $^{1}H-^{15}N$ NMR study of (1−71) bacterioopsin (a fragment of bacteriorhodopsin which contains TM helices A and B) solubilized in SDS revealed that most of the backbone amides participate

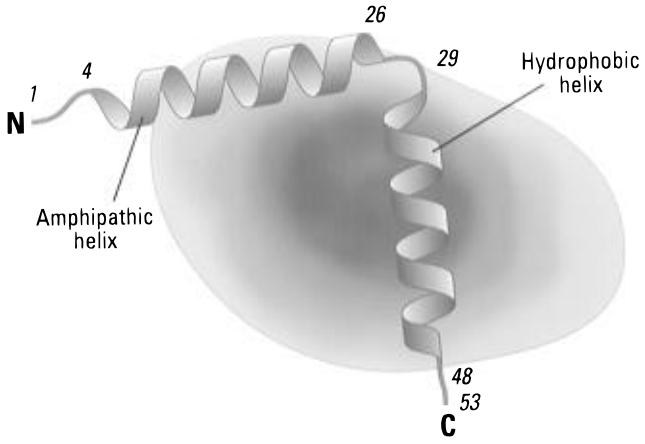

FIGURE 9: Schematic of the IKe coat protein in an MPG micelle. A dynamic model of micellar structure is employed rather than a static micelle (with explicit lysolipid molecules) to illustrate the transient nature of interactions between protein and lysolipid (excluding electrostatic interactions at the positively charged side chains). The core of the micelle is largely hydrophobic, with the mobility of the acyl chains creating an environment similar in density to a liquid hydrocarbon. The hydrophobic core is surrounded by a broad heterogeneous interfacial region which is composed of the lysolipid head group, acyl carbonyls, and acyl methylenes as well as water.

in conformational exchange processes with rates of 10^3-10^4 s^{-1} (order parameters of approximately 0.7) indicative of considerable motion between the two helices (Orekhov et al., 1994). The peaks from TM helices C, D, E, and F of bacteriorhodopsin in chloroform/methanol were missing from $^{1}H-^{15}N$ correlation spectra, an observation attributed to the conformational mobility of the four-helix bundle (Orekhov et al., 1992).

The conformational flexibility of the IKe coat protein may also reflect the requirement of the coat protein to undergo a conformational transition from the two-helix membrane-bound form to the extended single helix form upon assembly into the lipid-free virion. This transition has been described as a change in the tertiary structure of the protein with secondary structure being conserved (Shon et al., 1991). Many other proteins also occur in both membrane-bound and soluble forms including the colicins [e.g., Parker et al. (1994)] and defensins [e.g., Wimley and White (1994) and Cociancich et al. (1993)]. The transition between soluble and membrane-embedded forms depends upon the ability of the monomeric protein or complex to sequester the hydrophobic regions (exposed to the acyl chain environment in the membrane form) in the soluble protein. The interactions between the IKe coat protein and lipids in the membrane-bound form, and the coat protein, DNA, and other coat protein subunits in the virion, therefore reflect two alternative, thermodynamically favorable strategies to satisfy the structural requirements of the coat protein.

Summary. This study of the IKe coat protein in MPG micelles complements previous structural studies of the family of phage coat proteins (e.g., M13/fd and Pf1). The secondary structure of the IKe coat protein in an MPG micelle consists of two helical regions: a long N-terminal amphipathic helix (Asn 4−Ser 26) and a C-terminal helix (Trp 29−Phe 48) (Figure 9). The location of residues Thr 11−Ser 26 of the N-terminal amphipathic helix at the interface of the micelle was established by the observation of both lysolipid−protein NOEs and amide exchange with

water. Close contact between the micelle and residues 11−26 of the N-terminal helix is supported by the very similar relaxation properties observed for this part of the N-terminal helix and the C-terminal helix. The first 10 and last five residues of the IKe coat protein are mobile on very rapid time scales (i.e., picosecond). Motion between the two helices on much slower time scales (millisecond to microsecond) is likely and this is reflected by the requirement of R_{ex} terms to satisfy the relaxation data for many of the residues in the two helices. As well, slow exchange at the Trp 29 and Gln 27 positions was observed. The data are consistent with a range of values for the angle between the amphipathic and TM helices as opposed to a single fixed conformation. The features of the IKe coat protein consistent with the results presented here and with a large body of previous work on related systems (Shon et al., 1991; Henry & Sykes, 1992; van de Ven et al., 1993; McDonnell et al., 1993) are schematically illustrated in Figure 9. The coat protein is shown in the context of a dynamic model of the micelle, itself a fluid macromolecular assembly which fluctuates in both size and shape. This dynamic representation, rather than the use of explicit lysolipid molecules, emphasizes the largely transient nature of interactions between protein and lysolipid. This situation is supported experimentally by the occurrence of both amide exchange peaks and lysolipid acyl methylene NOEs to amide protons throughout much of the protein. In addition, however, specific interactions between detergent and protein also occur, as shown by the assignment of lysolipid head group NOEs to the side chains of positively charged residues. This study provides information regarding the secondary structure, dynamics and interactions between the IKe coat protein and its aqueous and micellar environments, which together allow for a detailed understanding of this model membrane protein.

ACKNOWLEDGMENT

We gratefully acknowledge the assistance of Ranjith Muhandiram and Guang-Yi Xu with NMR experiments.

SUPPORTING INFORMATION AVAILABLE

Two figures containing (1) $^{1}H-^{15}N$ HSQC of IKe in 400 mM ^{2}H-SDS and (2) decay and buildup curves arising from the slow exchange at Trp 29 and four tables containing (1) ^{15}N T_1, T_2, and NOE (500 MHz) and T_2 (600 MHz) relaxation values, (2) a summary of the analysis of relaxation data using a model free approach, (3) amide exchange rates and protection factors, and (4) chemical shift assignments (14 pages). Ordering information is given on any current masthead page.

REFERENCES

Abragam, A. (1961) *Principles of Nuclear Magnetism*, Clarendon Press, Oxford.

Attwood, D., & Florence, A. T. (1983) *Surfactant Systems. Their Chemistry, Pharmacy and Biology*, Chapman and Hall, London, U.K.

Bai, Y., Milne, J. S., Mayne, L., & Englander, S. W. (1993) *Proteins: Struct., Funct., Genet. 17*, 75−86.

Ballesteros, J. A., & Weinstein, H. (1992) *Biophys. J. 62*, 127.

Ben-Shaul, A., & Gelbart, W. M. (1994) in *Micelles, Membranes, Microemulsions, and Monolayers* (Gelbart, W. M., Ben-Shaul, A., & Roux, D., Eds.) Springer-Verlag, New York.

Bodenhausen, G., & Ruben, D. H. (1980) *Chem. Phys. Lett. 69*, 185−189.

Bogusky, M. J., Leo, G. C., & Opella, S. J. (1988) *Proteins: Struct., Funct., Genet. 4*, 123−130.

Brandts, J. F., Halvorson, H. R., & Brennan, M. (1975) *Biochemistry 14*, 4953−4963.

Cavanagh, J., & Rance, M. (1992) *J. Magn. Reson. 96*, 670−678.

Cavanagh, H., Palmer, A. G., Wright, P. E., & Rance, M. (1991) *J. Magn. Reson. 91*, 429−436.

Chazin, W. J., Kordel, J., Drakenberg, T., Thulin, E., Brodin, P., Grudstrom, T., & Forsen, S. (1989) *Proc. Natl. Acad. Sci. U.S.A. 86*, 2195−2198.

Clore, G. M., Szabo, A., Bax, A., Kay, L. E., Driscoll, P. C., & Gronenborn, A. M. (1990) *J. Am. Chem. Soc. 112*, 4989−4991.

Cociancich, S., Ghazi, A., Hetru, C., Hoffmann, J. A., & Letellier, L. (1993) *J. Biol. Chem. 268*, 19239−19245.

Cross, T. A., & Opella, S. J. (1979) *J. Supramol. Struct. 11*, 139−145.

Cross, T. A., & Opella, S. J. (1981) *Biochemisty 20*, 290−297.

Cross, T. A., & Opella, S. J. (1985) *J. Mol. Biol. 182*, 367−381.

Deber, C. M., Glibowicka, M., & Woolley, G. A. (1990) *Biopolymers 29*, 149−157.

Delaglio, F., Grzesiek, S., Vuister, G. W., Zhu, G., Pfeifer, J., & Bax, A. (1995) *J. Biomol. NMR 6*, 277−293.

Dunker, A. K., Ensign, L. D., Arnold, G. E., & Roberts, L. M. (1991) *FEBS Lett. 292*, 271−274.

Ellena, J. F., Hutton, W. C., & Cafiso, D. S. (1985) *J. Am. Chem. Soc. 107*, 1530−1537.

Farrow, N. A., Muhandiram, R., Singer, A. U., Pascal, S. M, Kay, C. M., Gish, G., Shoelson, S. E., Pawson, T., Forman-Kay, J. D., & Kay, L. E. (1994a) *Biochemistry 33*, 5984−6003.

Farrow, N. A., Zhang, O., Forman-Kay, J. D., & Kay, L. E. (1994b) *J. Biomol. NMR 4*, 727−734.

Farrow, N. A., Zhang, O., Forman-Kay, J. D., & Kay, L. E. (1995) *Biochemistry 34*, 868−878.

Garrett, D. S., Powers, R., Gronenborn, A. M., & Clore, G. M. (1991) *J. Magn. Reson. 95*, 214−220

Griesinger, C., Otting, G., Wüthrich, K., & Ernst, R. R. (1988) *J. Am. Chem. Soc. 110*, 7870−7873.

Gronenborn, A. M., & Clore, G. M. (1994) *J. Biomol. NMR 4*, 455−458.

Grzesiek, S., & Bax, A. (1992) *J. Am. Chem. Soc. 114*, 6291−6293.

Grzesiek, S., & Bax, A. (1993) *J. Am. Chem. Soc. 115*, 12593−12594.

Harper, E. T., & Rose, G. D. (1993) *Biochemistry 32*, 7605−7609.

Henry, G. D., & Sykes, B. D. (1990) *Biochem. Cell Biol. 68*, 318−329.

Henry, G. D., & Sykes, B. D. (1992) *Biochemistry 31*, 5284−5297.

Henry, G. D., & Sykes, B. D. (1994) *Methods Enzym*ol. *239*, 515−535.

Henry, G. D., Weiner, J. H., & Sykes, B. D. (1986) *Biochemistry 25*, 590−598.

Ikura, M., Kay, L. E., & Bax, A. (1990) *Biochemistry 29*, 4659−4667.

Jacobs, R. E., & White, S. E. (1989) *Biochemistry 28*, 3421−3437.

Kay, L. E. (1993) *J. Am. Chem. Soc. 115*, 2055−2057.

Kay, L. E., Torchia, D. A., & Bax, A. (1989) *Biochemistry 28*, 8972−8979.

Kay, L. E., Ikura, M., Tschudin, R., & Bax, A. (1990) *J. Magn. Reson. 89*, 496−514.

Kay, L. E., Keifer, P., & Saarinen, T. (1992) *J. Am. Chem. Soc. 114*, 10663−10665.

Kay, L. E., Xu, G. Y., Singer, A. U., Muhandiram, D. R., & Forman-Kay, J. D. (1993) *Magn. Res. Series B 101*, 333−337.

Kay, L. E., Xu, G. Y., & Yamazaki, T. (1994) *J. Magn. Reson. Ser. A 109*, 129−133.

Landolt-Marticorena, C., Williams, K. A., Deber, C. M., & Reithmeier, R. A. F. (1993) *J. Mol. Biol. 229*, 602−608.

Lee, W., Revington, M. J., Arrowsmith, C., & Kay, L. E. (1994) *FEBS Lett. 350*, 87−90.

Leo, G. C., Colnago, L. A., Valentine, K. G., & Opella, S. J. (1987) *Biochemistry 26*, 854−862.

Lipari, G., & Szabo, A. (1982a) *J. Am. Chem. Soc. 104*, 4546−4558.

Lipari, G., & Szabo, A. (1982b) *J. Am. Chem. Soc. 104*, 4559−4570.

MacArthur, M. W., & Thornton, J. M. (1991) *J. Mol. Biol. 218*, 397−412.
Marion, D., Kay, L. E., Sparks, S. W., Torchia, D. A., & Bax, A. (1989a) *J. Am. Chem. Soc. 111*, 1515−1517.
Marion, D., Driscoll, P. C., Kay, L. E., Wingfield, P. T., Bax, A., Gronenborn, A. M., & Clore, G. M. (1989b) *Biochemistry 28*, 6150−6156.
Marion, D., Ikura, M., Tschudin, R., & Bax, A. (1989c) *J. Magn. Reson. 85*, 393−399.
Marion, D., Ikura, M., & Bax, A. (1989d) *J. Magn. Reson. 84*, 425−430.
McCoy, M., & Mueller, L. (1992) *J. Am. Chem. Soc. 114*, 2108−2110.
McDermott, G., Prince, S. M., Freer, A. A., Hawthornthwaite-Lawless, A. M., Papiz, M. Z., Cogdell, R. J., & Isaacs, N. W. (1995) *Nature 374*, 517−519.
McDonnell, P. A., & Opella, S. J. (1993) *J. Magn. Reson. Ser. B 1*, 120−125.
McDonnell, P. A., Shon, K., Kim, Y., & Opella, S. J. (1993) *J. Mol. Biol. 233*, 447−463.
Muhandiram, D. R., & Kay, L. E. (1994) *J. Magn. Reson., Ser. B. 103*, 203−216.
Muhandiram, D. R., Farrow, N., Xu, G. Y., Smallcombe, S. H., & Kay, L. E. (1993) *J. Magn. Reson., Ser. B 102*, 317−321.
Opella, S. J., Kim, Y., & McDonnell, P. (1994) *Methods Enzym*ol *239*, 536−560.
Orekhov, V. Y., Abdulaeva, G. V., Musina, L. Y., & Arseniev, A. S. (1992) *Eur. J. Biochem. 210*, 223−229.
Orekhov, V. Y., Pervushin, K. V., & Arseniev, A. S. (1994) *Eur. J. Biochem. 219*, 887−896.
Palmer, A. G., Cavanagh, J., Wright, P. E., & Rance, M. (1991) *J. Magn. Reson. 93*, 151−170.
Papavoine, C. H. M., Konings, R. N. H., Hilbers, C. W., & van de Ven, F. J. M. (1994) *Biochemistry 33*, 12990−12997.
Parker, M. W., Buckley, J. T., Postma, J. P. M., Tucker, A. D., Leonard, K., Pattus, F., & Tsernoglou, D. (1994) *Nature 367*, 292−295.
Pascal, S., Muhandiram, D. R., Yamazaki, T., Forman-Kay, J. D., & Kay, L. E. (1994) *J. Magn. Reson. Ser. B 103*, 197−201.
Richardson, J. S., & Richardson, D. C. (1988) *Science 240*, 1548−1652.
Sambrook, J., Fritsch, E. F., & Maniatis, T. (1989) *Molecular Cloning: A Laboratory Manual*, 2nd ed., Cold Spring Harbor Laboratory, Cold Spring Harbor, NY.
Schleucher, J., Sattler, M., & Griesinger, C. (1993) *Angew. Chem., Int. Ed. Engl. 32*, 1489−1491.
Shaka, A. J., Keeler, J., Frenkiel, T., & Freeman, R. (1983) *J. Magn. Reson. 52*, 335−338.
Shaka, A. J., Barker, P., & Freeman, R. (1985) *J. Magn. Reson. 64*, 547−552.
Shon, K.-J., Kim, Y., Colnago, L. A., & Opella, S. J. (1991) *Science 252*, 1303−1305.
Stewart, D. E., Sarkar, A., & Wampler, J. E. (1990) *J. Mol. Biol. 214*, 253−260.
Stonehouse, J., Shaw, G. L., Keeler, H., & Laue, E. D. (1994) *J. Magn. Reson. Ser. A 107*, 178−184.
van de Ven, F. J. M., van Os, J. W. M., Aelen, J. M. A., Wymenga, S. S., Remerosski, M. L., Konings, R. N. H., & Hilbers, C. W. (1993) *Biochemistry 32*, 8322−8328.
Veis, A., & Nawrot, C. F. (1970) *J. Am. Chem. Soc. 92*, 3910−3914.
von Heijne, G. (1994) *Annu. Rev. Biophys. Biomol. Struct. 23*, 167−192.
Weiner, M. C., & White, S. H. (1992) *Biophys. J. 61*, 434−447.
White, S. H., & Wimley, W. C. (1993) *Curr. Opin. Struct. Biol. 4*, 79−86.
Williams, K. A., & Deber, C. M. (1993) *Biochem. Biophys. Res. Commun. 196*, 1−6.
Williams, K. A., & Deber, C. M. (1996) *Biochemistry* (submitted).
Williams, R. W., & Dunker, A. K. (1977) *J. Biol. Chem. 252*, 6253−6255.
Wimley, W. C., & White, S. H. (1993) *Biochemistry 32*, 6307−6312.
Wishart, D. S., & Sykes, B. D. (1994) *Methods Enzymol. 239*, 363−391.
Wishart, D. S., Sykes, B. D., & Richards, F. M. (1992) *Biochemistry 31*, 1647−1651.
Wishart, D. S., Bigam, C. G., Holm A., Hodges, R. S., & Sykes, B. D. (1995) *J. Biomol. NMR 5*, 67−81.
Wittekind, M., & Mueller, L. (1993) *J. Magn. Reson. Ser. B 101*, 201−205.
Zhang, O., Kay, L. E. Olivier, J. P., & Forman-Kay, J. D. (1994) *J. Biomol. NMR 4*, 845−858.
Zhu, G., & Bax, A. (1990) *J. Magn. Reson. 90*, 405−410.
Zhu, G., & Bax, A. (1992) *J. Magn. Reson. 100*, 202−207.
Zuiderweg, E. R. P., & Fesik, S. W. (1989) *Biochemistry 28*, 2387−2391.

BI952897W